doi:10.1093/brain/awaa266 BRAIN 2020: 143; 3343–3351 | 3343

BRAIN
A JOURNAL OF NEUROLOGY

Neuropathological correlates of cortical superficial siderosis in cerebral amyloid angiopathy

Andreas Charidimou,[1,2] Valentina Perosa,[1] Matthew P. Frosch,[3] Ashley A. Scherlek,[4] Steven M. Greenberg[1] and Susanne J. van Veluw[1,4]

Cortical superficial siderosis is an established haemorrhagic neuroimaging marker of cerebral amyloid angiopathy. In fact, cortical superficial siderosis is emerging as a strong independent risk factor for future lobar intracerebral haemorrhage. However, the underlying neuropathological correlates and pathophysiological mechanisms of cortical superficial siderosis remain elusive. Here we use an *in vivo* MRI, *ex vivo* MRI, histopathology approach to assess the neuropathological correlates and vascular pathology underlying cortical superficial siderosis. Fourteen autopsy cases with cerebral amyloid angiopathy (mean age at death 73 years, nine males) and three controls (mean age at death 91 years, one male) were included in the study. Intact formalin-fixed cerebral hemispheres were scanned on a 3 T MRI scanner. Cortical superficial siderosis was assessed on *ex vivo* gradient echo and turbo spin echo MRI sequences and compared to findings on available *in vivo* MRI. Subsequently, 11 representative areas in four cases with available *in vivo* MRI scans were sampled for histopathological verification of MRI-defined cortical superficial siderosis. In addition, samples were taken from predefined standard areas of the brain, blinded to MRI findings. Serial sections were stained for haematoxylin and eosin and Perls' Prussian blue, and immunohistochemistry was performed against amyloid-β and GFAP. Cortical superficial siderosis was present on *ex vivo* MRI in 8/14 cases (57%) and 0/3 controls ($P = 0.072$). Histopathologically, cortical superficial siderosis corresponded to iron-positive haemosiderin deposits in the subarachnoid space and superficial cortical layers, indicative of chronic bleeding events originating from the leptomeningeal vessels. Increased severity of cortical superficial siderosis was associated with upregulation of reactive astrocytes. Next, cortical superficial siderosis was assessed on a total of 65 Perls'-stained sections from MRI-targeted and untargeted sampling combined in cerebral amyloid angiopathy cases. Moderate-to-severe cortical superficial siderosis was associated with concentric splitting of the vessel wall (an advanced form of cerebral amyloid angiopathy-related vascular damage) in leptomeningeal vessels ($P < 0.0001$), but reduced cerebral amyloid angiopathy severity in cortical vessels ($P = 0.048$). In terms of secondary tissue injury, moderate-to-severe cortical superficial siderosis was associated with the presence of microinfarcts ($P = 0.025$), though not microbleeds ($P = 0.973$). Collectively, these data suggest that cortical superficial siderosis on MRI corresponds to iron-positive deposits in the superficial cortical layers, representing the chronic manifestation of bleeding episodes from leptomeningeal vessels. Cortical superficial siderosis appears to be the result of predominantly advanced cerebral amyloid angiopathy of the leptomeningeal vessels and may trigger secondary ischaemic injury in affected areas.

1 J. Philip Kistler Stroke Research Center, Department of Neurology, Massachusetts General Hospital, Harvard Medical School, Boston, MA, USA
2 Boston Medical Center, Boston University, Boston, MA, USA
3 Neuropathology Service, C.S. Kubik Laboratory for Neuropathology, Massachusetts General Hospital, Harvard Medical School, Boston, MA, USA
4 MassGeneral Institute for Neurodegenerative Disease, Massachusetts General Hospital, Charlestown, MA, USA

Received February 11, 2020. Revised May 25, 2020. Accepted June 29, 2020. Advance access publication September 16, 2020

Correspondence to: Susanne J. van Veluw, PhD
175 Cambridge Street, Boston 02114, MA, USA
E-mail: svanveluw@mgh.harvard.edu

Keywords: cerebral amyloid angiopathy; cortical superficial siderosis; magnetic resonance imaging; microbleeds; microinfarcts

Abbreviations: CAA = cerebral amyloid angiopathy; cSS = cortical superficial siderosis

Introduction

Cerebral amyloid angiopathy (CAA) is an age-related cerebral small vessel disease, characterized by the accumulation of amyloid-β in the walls of pial arteries and cortical perforators (Gilbert and Vinters, 1983). CAA is a frequent neuropathological observation in the brains of older individuals and is associated with cognitive impairment (Arvanitakis *et al.*, 2011). Clinically, CAA manifests itself on brain MRI by the occurrence of intracerebral haemorrhages (Greenberg and Charidimou, 2018). Traditionally, two forms of bleeding have been recognized in patients with CAA: large symptomatic lobar intracerebral haemorrhage and silent lobar cerebral microbleeds (Knudsen *et al.*, 2001).

More recently, a third form of bleeding has been identified in patients with CAA: cortical superficial siderosis (cSS) (Linn *et al.*, 2008, 2010). CSS is believed to be the chronic manifestation of episodes of acute convexity subarachnoid haemorrhage and can be identified on T_2*-weighted gradient echo or susceptibility-weighted imaging as focal or disseminated areas of signal loss following the gyral cortical surfaces in a curvilinear pattern (Charidimou *et al.*, 2015). CSS is associated with clinical symptoms in CAA, including transient focal neurological episodes (Greenberg *et al.*, 1993; Charidimou *et al.*, 2012), and is emerging as a strong independent risk factor for future lobar intracerebral haemorrhage (Linn *et al.*, 2010; Charidimou *et al.*, 2013*a*, 2019*a*). As such, cSS is now accepted as a key haemorrhagic neuroimaging signature in CAA and an important prognostic risk factor for future bleeding events in this patient population.

Nevertheless, the neuropathological correlates and potential underlying pathophysiological mechanisms of cSS remain poorly understood. Two possible pathways have been proposed through which cSS predicts worse outcome: (i) cSS may reflect particularly severe CAA in the leptomeningeal vessels, thereby identifying individuals with more advanced disease; or (ii) cSS may directly predispose vessels to rebleed, potentially through secondary tissue injury in the underlying cortex. To address these outstanding questions, we performed a high-resolution post-mortem MRI-histopathology correlation study in CAA cases with available clinical *in vivo* MRI scans. In this unique dataset we assessed the neuropathological correlates of cSS and explored potential mechanisms of secondary tissue injury.

Materials and methods

Cases

Fifteen consecutive autopsy cases with a clinical diagnosis of possible or probable CAA that consented to brain donation were included from an ongoing brain autopsy program initiated in 2015 within the haemorrhagic stroke research group at the Massachusetts General Hospital (MGH) (Van Veluw *et al.*, 2019*a*). This program aims to evaluate MRI markers and their underlying histopathology in the context of CAA. Cases were either received through MGH or from outside hospitals. Medical records and available *in vivo* clinical MRI scans were requested for each case and evaluated for the presence and severity of cSS by an experienced rater (A.C.), according to previously proposed rating criteria (Charidimou *et al.*, 2015). At autopsy, brains were extracted and fixed in 10% formalin, after which the hemispheres were separated. One intact hemisphere was subjected to *ex vivo* 3 T MRI scanning and histopathological examination. The other hemisphere underwent routine neuropathological examination following standardized protocols. One case proved not to have CAA on neuropathology and hence was considered a control case in this study going forward (CTRL Case 3 in Table 1). In addition, intact hemispheres from two consecutive control cases without neurological conditions or CAA on neuropathology were included from the MGH neuropathology service.

Ex vivo MRI scanning

Prior to scanning, each hemisphere was vacuum-sealed in a plastic bag containing periodate-lysine-paraformaldehyde and scanned as described previously (Van Veluw *et al.*, 2019*a*). Briefly, each packed hemisphere was placed in the 32-channel head coil of a whole-body 3 T MRI scanner (MAGNETOM Trio, Siemens Healthineers) and scanned with an overnight protocol. The sequences relevant for the current study included a T_2-weighted turbo-spin echo (TSE) sequence (echo time 61 ms, repetition time 1800 ms, flip angle 150°, voxel size $500 \times 500 \times 500$ μm^3, one average, total scan time ~3 h), and a T_2*-weighted dual echo gradient-echo fast low angle shot (FLASH) sequence (echo times 4.49 ms and 11.02 ms, repetition time 20 ms, flip angles 10°, 20°, 30°, voxel size $500 \times 500 \times 500$ μm^3, two averages, total scan time ~2 h).

Ex vivo MRI assessment

Scans were processed in FreeSurfer (https://surfer.nmr.mgh.harvard.edu) to obtain 3D volumes. Presence of cSS was assessed on the TSE and FLASH scans by two experienced raters (A.C.

Table 1 Case characteristics

Case ID	Gender	Age at death, years	Death due to acute ICH	PMI, h	*In vivo* MRI and death interval, months	cSS on *in vivo* MRI	cSS on *ex vivo* MRI	Cumulative CAA severity score[a] (cortical/ leptomeningeal)	Other neuropathological observations[b]
Cases									
1	Male	80	No	Unknown	86.8	Yes (disseminated)	Yes	5 / 6	A3B3C2
2	Male	70	Yes	16	n/a	n/a	Yes	9 / 5	A3B3C1
3	Male	76	No	27	18.9	Yes (disseminated)	Yes	7 / 8	A3B3C2
4	Male	65	Yes	14	8.1	No	No	7 / 7	A3B1C2
5	Male	81	No	Unknown	0.2	Yes (focal)	Yes	5 / 7	A3B2C2
6	Female	70	Yes	Unknown	13.7	Yes (disseminated)	Yes	6 / 11	A3B1C1
7	Male	67	No	Unknown	15.7	No	No	10 / 8	A3B3C2
8	Male	69	Yes	36	6.3	No	Yes	10 / 11	A3B1C2
9	Female	64	Yes	30	61.1	No	No	8 / 11	A3B2C3
10	Female	79	Yes	37	101.8	No	No	8 / 11	A3B3C2
11	Male	67	No	24	17.2	Yes (disseminated)	Yes	5 / 12	A3B1C1
12	Female	88	Yes	11	8.0	No	Yes	8 / 9	A2B3C2
13	Female	67	No	15	5.3	No	No	10 / 11	A3B3C3
14	Male	85	No	18	7.1	No	No	1 / 4	A3B3C3
Controls									
1	Male	90	No	6	n/a	n/a	No	0 / 1	A2B1C2
2	Female	95	No	4	79.1	No	No	0 / 2	A1B2C0
3	Female	88	No	9	18.3	No	No	0 / 1	A2B1C1, globular glial tauopathy

[a]CAA severity was evaluated on the amyloid-β-stained sections from the predefined standard areas of frontal, temporal, parietal, and occipital cortex using a 4-point scale: absent (0); scant amyloid-β deposition (1); some circumferential amyloid-β (2); widespread circumferential amyloid-β (3), following proposed consensus criteria (Love *et al.*, 2014). Scores were determined separately for the cortical vessels and the leptomeningeal vessels from the four areas and were separately added to form a cumulative CAA severity score.
[b]Extracted from neuropathology reports, based on routine neuropathological examination. ABC score reflects the NIA-Alzheimer Association score for Alzheimer's Disease neuropathological changes (Hyman *et al.*, 2012).
ICH = intracerebral haemorrhage; n/a = not available; PMI = post-mortem interval.

and S.J.v.V.) and defined as presence of well-defined, homogeneous hypointense curvilinear black signal intensity in the superficial layers of the cortex, within the subarachnoid space, or both (Charidimou *et al.*, 2015). The cerebellum was excluded from the assessment.

Histopathology

After scanning, the brains were cut into 1-cm thick coronal slabs. Representative areas with MRI-defined cSS were sampled for histopathological verification. In addition, samples were taken from predefined standard areas of the frontal, temporal, parietal, and occipital lobe, blinded to MRI. All sampled tissue blocks were processed and embedded in paraffin, after which several 6-µm thick serial sections were cut on a microtome. Haematoxylin and eosin and Perls' Prussian blue staining were performed using standard histology protocols. For the Perls' protocol sections were incubated with a 1:1 mixture of 5% hydrochloric acid and 5% potassium ferrocyanide (30 min), and counterstained with filtered neutral red (1 min). On adjacent sections, bright field immunohistochemistry against amyloid-β (mouse, clone 6F/3D, Agilent, 1:200) and GFAP (rabbit, G9269, Sigma, 1:1000) was performed as described previously (Van Veluw *et al.*, 2019*b*). Briefly, after deparaffinization, endogenous peroxidase was blocked with 3% H_2O_2 (20 min), followed by formic acid treatment (only for amyloid-β, 5 min) or heated citrate buffer (only for GFAP, 20 min). Sections were blocked with normal serum (1 h) and incubated with the primary antibody overnight at 4°C. The next day, a biotinylated secondary antibody was applied (Vectastain ABC kit, Vector laboratories, 1 h) followed by an incubation with a mixture of avidin and biotinylated HRP (Vectastain ABC kit, 30 min), and 3,3′-diaminobenzidine (5 min).

Histopathological image analysis

Each stained section was scanned with a Hamamatsu NanoZoomer Digital Pathology (NDP)-HT whole slide scanner (C9600-12, Hamamatsu Photonics KK), using a 20× objective. The digital images were rated in the software NDP.View2 (version 2.7.25). Presence and severity of iron-positive (blue) deposits in the subarachnoid space and cortical layers was assessed by two experienced raters (A.C. and S.J.v.V.) in consensus, on each individual Perls' Prussian blue-stained section as absent (0), mild (1), moderate (2), or severe (3) (Supplementary Fig. 1). In addition, the adjacent haematoxylin and eosin-stained sections were assessed to verify the presence of haemosiderin (honey brown) deposits. CAA severity was assessed on amyloid-β-stained sections using a 4-point scale; absent (0), scant amyloid-β deposition (1), some circumferential amyloid-β (2), and widespread circumferential amyloid-β (3), following proposed consensus criteria with minor modifications (Love *et al.*, 2014), blinded to cSS severity. In addition, vessel-within-vessel pathology (i.e. concentric splitting of the vessel wall) was determined as absent (0), occasional vessel (1), or many vessels (2). Scores were determined separately for the cortical and the leptomeningeal vessels (Supplementary Fig. 2). Upregulation of reactive astrocytes in the superficial layers of the cortex was determined on the

GFAP-stained sections (yes/no), blinded to cSS severity. To determine inter-rater reliability for each histopathological measure, 30% of the sections were scored by a third independent blinded rater (V.P.). Presence and number of cortical microbleeds and microinfarcts were assessed on haematoxylin and eosin-stained sections, following published criteria (Van Veluw *et al.*, 2019*b*). Finally, parenchymal amyloid-β plaque severity was assessed using a 4-point scale; absent (0), mild (1), moderate (2), severe (3) by two independent raters (S.J.v.V. and V.P.), followed by a consensus rating to obtain a final score.

In addition, to perform a more quantitative assessment of cSS and astrogliosis, digital images of the Perls' and GFAP-stained sections were uploaded to the Aiforia™ image processing and management platform (Aiforia Technologies) for analysis with deep learning convolution neural networks and supervised learning. Two separate multi-layered convolution neural networks were trained on tissue and positive cell annotations from a representative subset of images. After refining the final AI model, the algorithm was applied to the frontal lobe sections of all CAA cases and controls after manually outlining the cortical ribbon to obtain the number of iron-positive deposits and GFAP-positive astrocytes (Supplementary Fig. 3).

Statistical analysis

A chi-square test was performed to compare proportions of cases and controls with and without cSS on MRI. The relationship between density of iron-positive deposits and reactive astrocytes (number of detections/mm^2 tissue) within the cortex was assessed with Spearman correlations. Presence of cSS (i.e. mild-to-severe) versus absence on histopathology was compared between CAA cases and controls using a chi-square test for proportions. Inter-rater reliability for each histopathological measure was assessed using the intra-class correlation coefficient (ICC) and revealed good to excellent agreement between independent raters (median ICC for all measures assessed 0.9, range 0.777–0.984). Within CAA cases, cSS severity was dichotomized (i.e. absent-to-mild versus moderate-to-severe) after which histopathological measures were compared using chi-square tests for proportions. Multivariable logistic regression models were also performed to explore associations with cSS presence and severity and CAA pathology, adjusted for age at death, case ID, and anatomical area. A *P*-value of <0.05 was considered statistically significant. Analyses were done in IBM SPSS v.22 and STATA v.13.

Data availability

Data can be made available by the corresponding author upon reasonable request.

Results

Histopathology of cortical superficial siderosis

Fourteen cases with CAA (mean age at death 73 ± 8 years, nine males) and three controls (mean age at death 91 ± 4 years, one male) were included in this study. Clinical *in vivo* MRI scans were available for 13/14 cases, acquired on average 26.9 months prior to death (median 13.7, range 0.2–101.8 months), and 2/3 controls, acquired 18.3 and 79.1 months prior to death respectively. On the *in vivo* MRI scans, cSS was present in 5/13 cases (38%), as focal in one and disseminated in four, and none of the two controls (Table 1).

On the *ex vivo* MRI scans of the intact hemispheres cSS was present in 8/14 cases (57%) and 0/3 controls (0%, $P = 0.072$). Eleven representative samples from four cases with available *in vivo* MRI scans (Cases 1, 3, 6, and 11) were taken from areas with cSS. For 10/11 samples, cSS was present in the targeted areas on both *in vivo* and *ex vivo* MRI, whereas for 1/11 samples cSS was only visible on the *ex vivo* MRI. The histopathology in the 10 areas revealed iron-positive haemosiderin deposits in the subarachnoid space and superficial cortical layers (layers I–III) of varying degrees across all samples (median iron score 3, range 1–3). Within the cortex, iron deposits were mainly found across layers I–III both extracellularly and engulfed by macrophages. Iron was only occasionally found in neurons and infrequently extended into the deeper layers (IV–VI) of the cortex (Fig. 1).

Notably, for the sample with cSS on *ex vivo* MRI but not *in vivo* MRI, fresh blood was observed in the subarachnoid space upon gross examination. The histopathology revealed only mild degree of iron-positive deposits, with no cortical involvement, but many intact red blood cells were present in the subarachnoid space, indicative of a recent bleeding event (Fig. 2).

Collectively, we observed that the degree and pattern of cSS on *ex vivo* MRI corresponded closely with the degree and pattern of the iron deposits on histopathology, both in terms of severity and extend of cortical involvement. Moreover, increased iron deposition was associated with upregulation of reactive astrocytes in the same cortical areas (Fig. 2). AI-guided quantitative assessment of the frontal cortex revealed that the number of iron-positive deposits was positively correlated with the number of reactive astrocytes (Spearman's ρ 0.686, $P = 0.002$).

Vascular basis of cortical superficial siderosis

Next, cSS severity was assessed on iron-stained sections on samples taken from the predefined standard areas of the frontal, temporal, parietal, and occipital lobe, blinded to MRI ($n = 56$ sections in 14 cases and $n = 12$ sections in three controls). In the CAA cases, iron deposits were present in 25/56 sections (45%) and was scored as moderate-to-severe in 10/56 sections (18%). In the controls, no iron deposits were observed in any of the 12 sections ($P = 0.004$).

Although we screened sections for evidence of ruptured vessels, no sites of (recent or old) bleeding could be identified either at the level of the leptomeningeal or cortical blood vessels. Based on all MRI-targeted and -untargeted sections

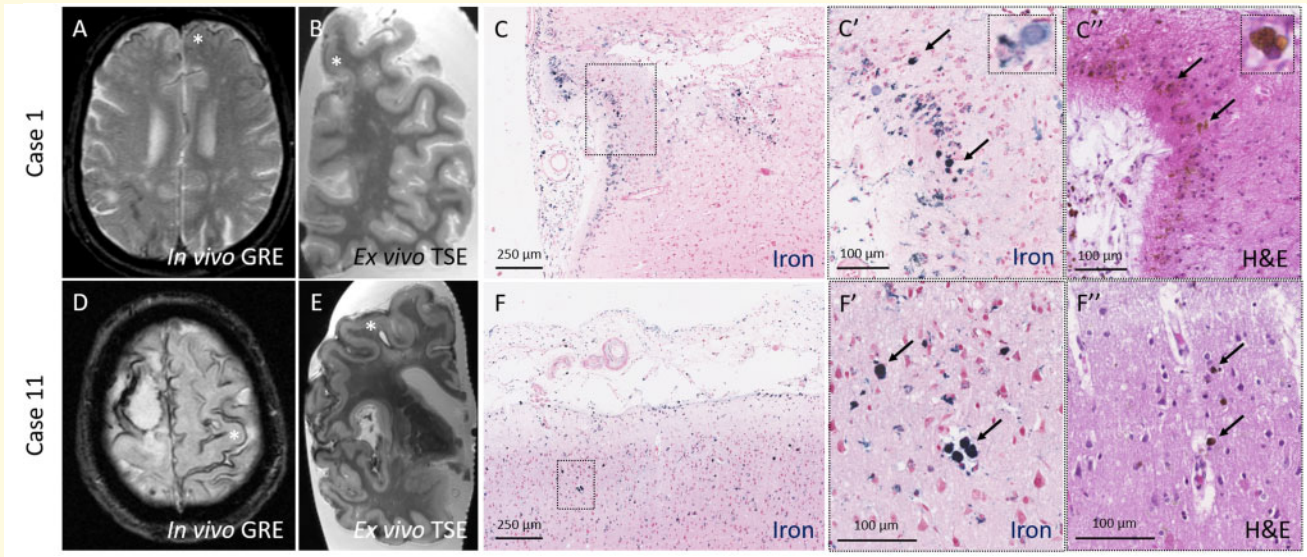

Figure 1 Histopathological verification of cSS observed on *in vivo* MRI in CAA cases. *Top row*: CSS (asterisk) was observed on an *in vivo* gradient echo MRI scan performed ~7 years prior to death in an individual with a clinical diagnosis of probable CAA (Case 1) (**A**). On the *ex vivo* turbo spin echo MRI scan the same area was positive for cSS (**B**, asterisk). On the corresponding histopathological section, iron-positive deposits were observed in the subarachnoid space and superficial layers of the cortex (**C**). The *insets* reveal greater detail of the intracellular iron deposits (**C′**, arrows), corresponding to haemosiderin-containing macrophages on the adjacent haematoxylin and eosin-stained section (**C″**, arrows). *Bottom row*: Disseminated cSS (asterisk) was observed on an *in vivo* gradient echo MRI scan performed ~1.5 years prior to death in an individual with a clinical diagnosis of probable CAA (Case 11) (**D**). On the *ex vivo* turbo spin echo MRI scan the same area was positive for cSS (**E**, asterisk) (note the same enlarged perivascular space on the *in vivo* and *ex vivo* scan). On the corresponding histopathological section, iron-positive deposits were observed in the subarachnoid space and superficial layers of the cortex (**F**). The *insets* reveal greater detail of the intracellular iron deposits (**F′**, arrows), corresponding to haemosiderin-containing macrophages on the adjacent haematoxylin and eosin-stained section (**F″**, arrows). GRE = gradient echo; H&E = haematoxylin and eosin; TSE = turbo spin echo.

within the CAA cases combined (total $n = 65$ sections), moderate-to-severe cSS on iron-stained sections was associated with increased CAA severity in leptomeningeal vessels ($P = 0.072$), but reduced severity in cortical vessels ($P = 0.048$). The strongest associations were found between cSS and leptomeningeal (though not cortical) vessel-within-vessel pathology ($P < 0.0001$) and upregulation of reactive astrocytes in the underlying cortex ($P = 0.001$). Parenchymal amyloid-β plaques were observed in almost all CAA cases, but there was no association between degree of cSS and amyloid-β plaque burden ($P = 0.401$) (Table 2).

In multivariable logistic regression models, cSS presence and severity remained strongly associated with leptomeningeal CAA and vessel-within-vessel pathology, independent of cortical CAA severity or anatomical area assessed (Fig. 3 and Supplementary Table 1).

Finally, we explored the association between cSS and presence of cortical microbleeds and microinfarcts on the same section in the total dataset ($n = 65$ samples). Fourteen microbleeds and 110 microinfarcts were observed on the haematoxylin and eosin-stained sections. Interestingly, moderate-to-severe cSS on iron-stained sections was associated with presence of microinfarcts ($P = 0.025$), though not microbleeds ($P = 0.973$) (Table 2 and Fig. 3).

Discussion

This combined *in vivo* MRI, *ex vivo* MRI, histopathology study revealed several key findings. We confirmed the neuropathological substrate of cSS as iron-positive haemosiderin deposits in the subarachnoid space and superficial layers of the cortex. Moreover, moderate-to-severe cSS was associated with moderate-to-severe leptomeningeal CAA and concentric splitting of the walls of leptomeningeal vessels, with a relative sparing of cortical vessels. This pattern is consistent with the notion that cSS represents the chronic manifestation of bleeding from the leptomeningeal vessels, as a result of advanced CAA. The presence of reactive astrocytes and cortical microinfarcts in the underlying cortical areas suggests that cSS may trigger secondary tissue injury, which could contribute to an increased bleeding risk in affected individuals.

Despite the lack of true longitudinal data, our combined cross-sectional analysis of both *in vivo* and *ex vivo* MRI findings followed by neuropathology suggests the following sequence of events to occur in cSS. Advanced CAA in the leptomeningeal vessels triggers subtle bleeding into the subarachnoid space, after which blood breakdown products are taken up and enter the superficial layers of the underlying cortex. This process is potentially mediated by an

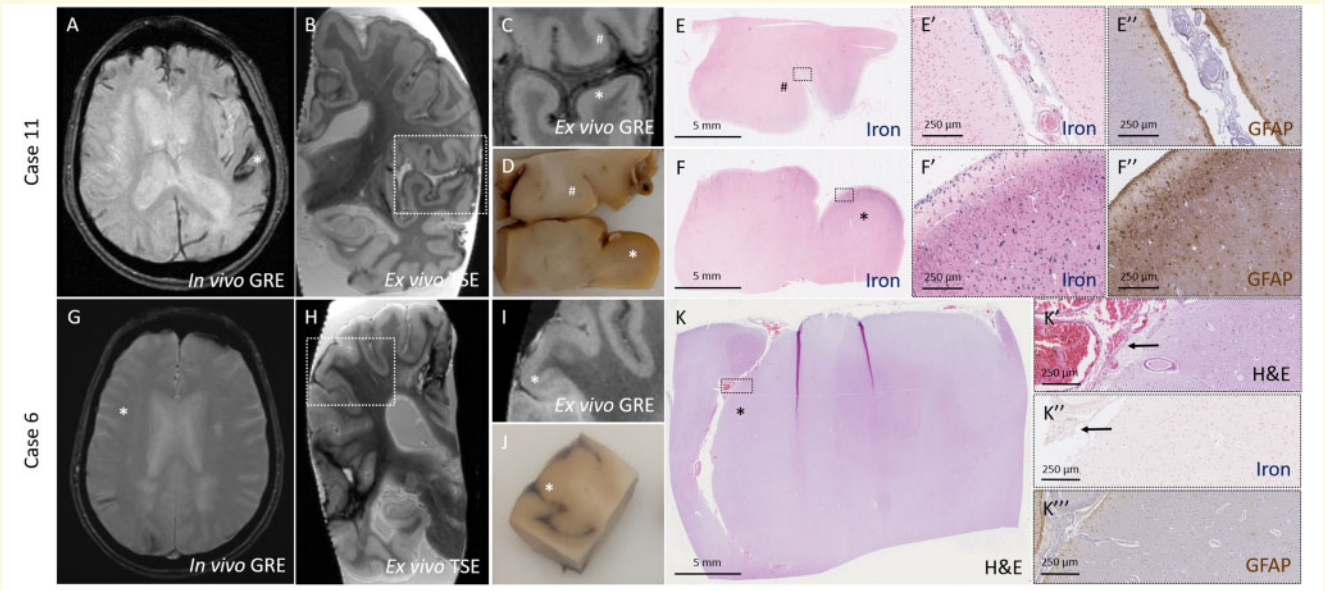

Figure 2 Degree and pattern of cSS on MRI closely corresponds to degree and pattern of iron-positive deposits on histopathology. *Top row*: CSS (asterisk) was observed on an *in vivo* gradient echo MRI scan performed ~1.5 years prior to death in an individual with a clinical diagnosis of probable CAA (Case 11) (**A**). On the *ex vivo* gradient echo scan varying degree of cSS can be observed (**B**), including subtle (number sign) and extensive (asterisk) hypointense signal (**C**). On gross examination of the formalin-fixed tissue, no visible alterations were observed in the area with subtle cSS (number sign), whereas orange discolouration was present in the superficial cortex in the area with extensive cSS (asterisk) (**D**). The degree of hypointense signal on MRI matched closely to the degree of iron-positive deposits on the corresponding histopathological sections (**E** and **F**). The *insets* reveal greater detail of the degree of iron deposits, which was subtle and restricted to the subarachnoid space and pial surface in **E′** and extensive and involving the superficial and deeper layers of the cortex in F′. Many reactive astrocytes were found in the area with extensive iron deposits (**F″**), but not in the area with subtle iron deposits (**E″**). *Bottom row*: No evidence of cSS was observed on *in vivo* gradient echo MRI performed ~1 year prior to death in an individual with a clinical diagnosis of probable CAA (Case 6) (**G**) in the area (asterisk) corresponding to an area with cSS on *ex vivo* turbo spin echo MRI (**H**). On the *ex vivo* gradient echo scan cSS is subtle and only observed in the subarachnoid space (asterisk) (**I**). On gross examination of the formalin-fixed tissue, fresh blood was observed in the subarachnoid space of the sulcus (asterisk) (**J**), corresponding to intact red blood cells on haematoxylin and eosin (**K**). The *insets* reveal greater detail of the red blood cells in **K′** (arrows), which were only mildly positive for iron (**K″**, arrows). No reactive astrocytes were found in this area (**K‴**). GRE = gradient echo; H&E = haematoxylin and eosin; TSE = turbo spin echo.

upregulation of reactive astrocytes. In the chronic stages, blood breakdown products seem to be stored long-term within cells (and occasionally neurons). Collectively, the localization and degree of iron as a result of bleeding from the surface vessels gives rise to the curvilinear intracortical pattern of hypointense signal on MRI, characteristic of cSS.

Clinically, cSS is the strongest predictor for future intracerebral haemorrhages in patients with CAA (Charidimou *et al.*, 2019*a*). A likely explanation is the strong association with severe CAA in the leptomeningeal vessels, which includes fragmentation of the vessel walls, seen on neuropathology as vessel-within-vessels. The significant association between moderate-to-severe cSS and reduced cortical CAA in the setting of advanced leptomeningeal CAA is interesting, as it suggests that a preferential distribution of amyloid-β towards the surface vessels gives rise to bleeding from those vessels. This process could be mediated by the apolipoprotein E (*APOE*) genotype, as recently suggested (Charidimou *et al.*, 2019*b*). *APOE* ε2 is associated with leptomeningeal CAA and cSS (i.e. bleeding from the surface vessels) (Schilling *et al.*, 2013; Pichler *et al.*, 2017; Charidimou *et al.*, 2019*b*), whereas *APOE* ε4 favours cortical CAA and cortical microbleeds (i.e. bleeding from penetrating cortical vessels) (Premkumar *et al.*, 1996; Poels *et al.*, 2010; Charidimou *et al.*, 2019*b*). In addition, this differential distribution of CAA pathology may reflect different clearance mechanisms of amyloid-β associated with different isoforms of APOE (Castellano *et al.*, 2011). Unfortunately, we did not have *APOE* status information available for the cases reported in this study to address the relationship between bleeding patterns and CAA distribution, an interesting topic for future studies. Since patients with cSS are at increased risk to develop large lobar intracerebral haemorrhages, our neuropathological observations raise the possibility that some of these larger bleeds may originate directly from leptomeningeal vessels. Noteworthy in this context are two published case reports of unrelated patients with a similar point mutation in the coding region of the *APP* gene, the Piedmont mutation (Obici *et al.*, 2005; Kozberg *et al.*, 2020). Both cases suffered from several large lobar intracerebral haemorrhages, in rapid succession, and proved to have remarkable advanced leptomeningeal CAA on

Table 2 Associations between cSS and pathology burden in CAA cases

Pathology assessed	Moderate-to-severe cSS (*n* = 18)	Absent-to-mild cSS (*n* = 47)	*P*-value
Moderate-to-severe cortical CAA	7 (39)	31 (66)	0.048
Moderate-to-severe leptomeningeal CAA	17 (94)	35 (74)	0.072
Many cortical vessel-within-vessels	0 (0)	3 (7)	0.272
Many leptomeningeal vessel-within-vessels	14 (78)	7 (15)	<0.0001
Moderate-to-severe parenchymal amyloid-β plaques	17 (94)	41 (87)	0.401
Reactive astrocytes presence	18 (100)	26 (55)	0.001
Microbleed presence	3 (17)	8 (17)	0.973
Microinfarct presence	14 (78)	22 (47)	0.025

Data are presented as *n* (%).

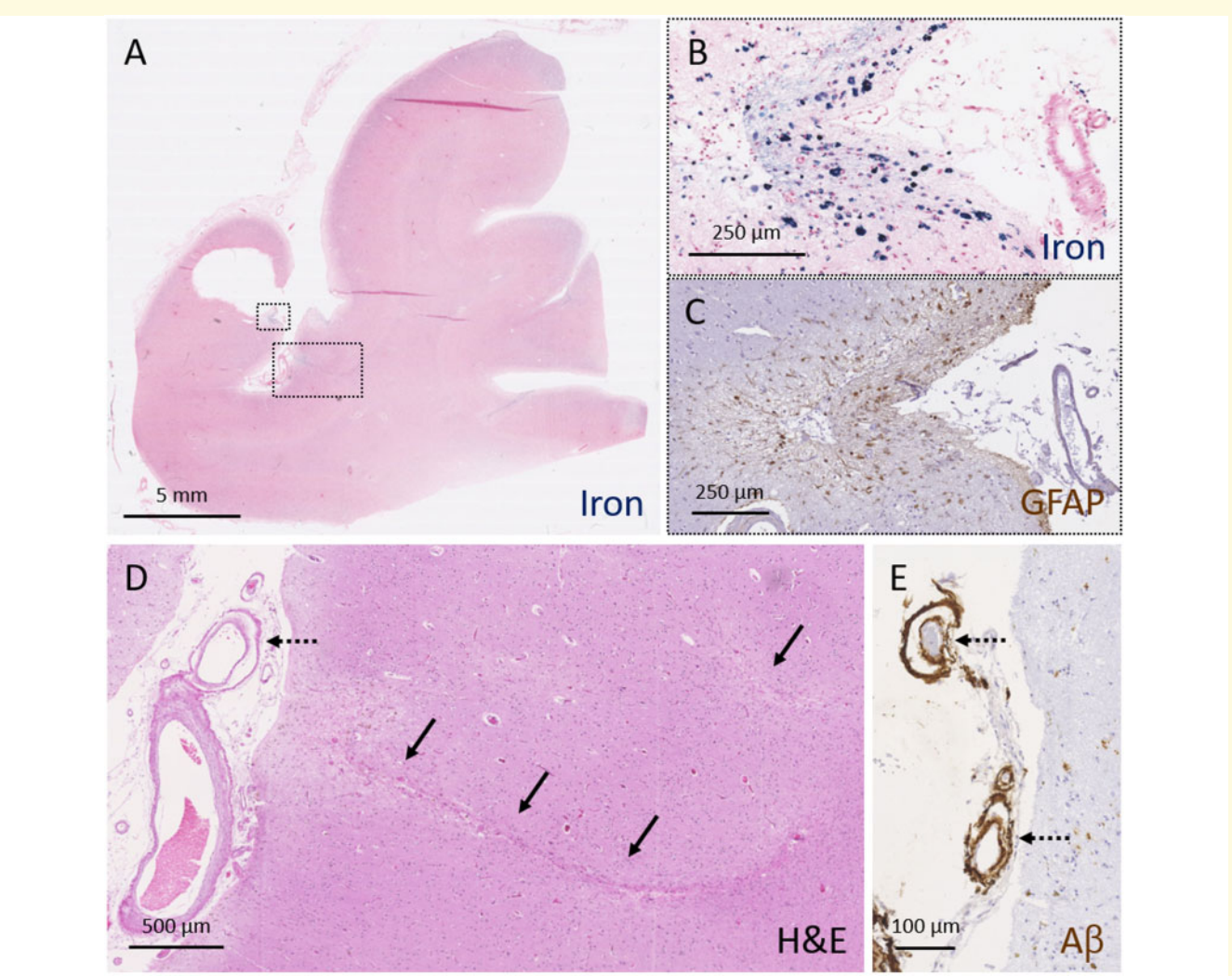

Figure 3 Moderate-to-severe cSS is associated with advanced leptomeningeal CAA and secondary tissue injury. A representative example of severe cSS as assessed on a Perls' Prussian blue-stained section (**A**). Higher magnification of the area outlined with the small box in A, reveals greater detail of severe cSS (**B**). An adjacent section stained for GFAP revealed many reactive astrocytes in the superficial cortical layers in this area (**C**). Two cortical microinfarcts (indicated with solid arrows) were observed in the neighbouring cortical area (**D**, area corresponds to larger box in **A**). Note the presence of vessel-within-vessel pathology (indicated with broken arrows) in combination with severe CAA of the leptomeningeal vessels (**D** and **E**). Aβ = amyloid-β; H&E = haematoxylin and eosin.

neuropathological examination of the brain post-mortem. Interestingly, the cortical vessels were relatively unaffected, which may have explained their preserved cognitive status reported during life and relative lack of cortical microvascular lesions (Kozberg *et al.*, 2020).

The significant association between moderate-to-severe cSS on pathology and the presence of cortical microinfarcts in our study suggests that cSS may trigger secondary tissue injury. Previous studies have also found a relationship between cSS and microinfarcts on *ex vivo* MRI (De Reuck *et al.*, 2013) and on *in vivo* MRI in patients with CAA (Van Veluw *et al.*, 2017; Xiong *et al.*, 2018). Importantly, reports of a spatial overlap between areas of cSS and microinfarcts on MRI are in line with our neuropathological observations (Beitzke *et al.*, 2018; Ii *et al.*, 2019). A potential underlying mechanism through which cSS may cause ischaemic tissue injury could be cortical spreading depolarizations (Hartings *et al.*, 2017). Cortical spreading depolarizations can occur after acute subarachnoid haemorrhages and may provide an intriguing explanation for the occurrence of transient focal neurological episodes in affected individuals (Charidimou *et al.*, 2013*b*). This link would also present the desirable opportunity for the development of much needed intervention strategies, as this clinical symptom may be amenable to medications.

The strength of this study is the availability of a unique dataset including whole brain high-resolution *ex vivo* MRI scans of well-characterized individuals with available *in vivo* MRI. Because of the inherent nature of post-mortem investigations, this study presents with several limitations. First, the time between *in vivo* MRI and death was heterogeneous, and precluded us from performing in-depth longitudinal analyses. Second, this dataset reflects a selective group of patients who participated in brain donation, which may not be generalizable to other (clinical) settings. Third, because of the extensive involvement of cSS we could not identify the individual leptomeningeal vessel (or several vessels) that had bled. In the future, this may be achieved by means of serial sectioning of relatively large areas, which is rather labour intensive. As of now, we cannot exclude potential other bleeding sources (e.g. remote large haemorrhages, haemorrhagic transformation of cortical microinfarcts). Future work is warranted to focus on the pathophysiology of cSS in the context of CAA and secondary tissue injury, using in-depth neuropathological assessments and experimental animal models.

Acknowledgements

The authors would like to thank Lindsey Smith and Andre van der Kouwe for excellent technical support.

Funding

This works was supported by the National Institute of Aging (K99 AG059893 to S.J.v.V. and R01 AG026484 to S.M.G.) and a Heitman Young Investigator Career Development Award (to S.J.v.V.).

Competing interests

The authors report no competing interests.

Supplementary material

Supplementary material is available at *Brain* online.

References

Arvanitakis Z, Leurgans SE, Barnes LL, Bennett DA, Schneider JA. Microinfarct pathology, dementia, and cognitive systems. Stroke 2011; 42: 722–7.

Beitzke M, Enzinger C, Pichler A, Wünsch G, Fazekas F. Acute diffusion-weighted imaging lesions in cerebral amyloid angiopathy-related convexal subarachnoid hemorrhage. J Cereb Blood Flow Metab 2018; 38: 225–9.

Castellano JM, Kim J, Stewart FR, Jiang H, DeMattos RB, Patterson BW, et al. Human apoE isoforms differentially regulate brain amyloid-β peptide clearance. Sci Transl Med 2011; 3: 89ra57.

Charidimou A, Baron JC, Werring DJ. Cerebral amyloid angiopathy and transient focal neurological episodes. Cerebrovasc Dis 2013b; 36: 245–6.

Charidimou A, Boulouis G, Greenberg SM, Viswanathan A. Cortical superficial siderosis and bleeding risk in cerebral amyloid angiopathy: a meta-analysis. Neurology 2019a; 93: e2192–e202.

Charidimou A, Linn J, Vernooij MW, Opherk C, Akoudad S, Baron JC, et al. Cortical superficial siderosis: detection and clinical significance in cerebral amyloid angiopathy and related conditions. Brain 2015; 138: 2126–39.

Charidimou A, Peeters A, Fox Z, Gregoire SM, Vandermeeren Y, Laloux P, et al. Spectrum of transient focal neurological episodes in cerebral amyloid angiopathy: multicentre magnetic resonance imaging cohort study and meta-analysis. Stroke 2012; 43: 2324–30.

Charidimou A, Peeters AP, Jäger R, Fox Z, Vandermeeren Y, Laloux P, et al. Cortical superficial siderosis and intracerebral hemorrhage risk in cerebral amyloid angiopathy. Neurology 2013a; 81: 1666–73.

Charidimou A, Zonneveld HI, Shams S, Kantarci K, Shoamanesh A, Hilal S, et al. APOE and cortical superficial siderosis in CAA: meta-analysis and potential mechanisms. Neurology 2019b; 93: e358–e71.

De Reuck J, Deramecourt V, Cordonnier C, Auger F, Durieux N, Pasquier F, et al. Superficial siderosis of the central nervous system: a post-mortem 7.0-tesla magnetic resonance imaging study with neuropathological correlates. Cerebrovasc Dis 2013; 36: 412–7.

Gilbert JJ, Vinters HV. Cerebral amyloid angiopathy: incidence and complications in the aging brain. I. Cerebral hemorrhage. Stroke 1983; 14: 915–23.

Greenberg SM, Charidimou A. Diagnosis of cerebral amyloid angiopathy: evolution of the Boston Criteria. Stroke 2018; 49: 491–7.

Greenberg SM, Vonsattel JP, Stakes JW, Gruber M, Finklestein SP. The clinical spectrum of cerebral amyloid angiopathy: presentations without lobar hemorrhage. Neurology 1993; 43: 2073–9.

Hartings JA, York J, Carroll CP, Hinzman JM, Mahoney E, Krueger B, et al. Subarachnoid blood acutely induces spreading depolarizations and early cortical infarction. Brain 2017; 140: 2673–90.

Hyman BT, Phelps CH, Beach TG, Bigio EH, Cairns NJ, Carrillo MC, et al. National Institute on Aging-Alzheimer's Association guidelines for the neuropathologic assessment of Alzheimer's disease. Alzheimers Dement 2012; 8: 1–13.

Knudsen KA, Rosand J, Karluk D, Greenberg SM. Clinical diagnosis of cerebral amyloid angiopathy: validation of the Boston criteria. Neurology 2001; 56: 537–9.

Kozberg MG, van Veluw SJ, Frosch MP, Greenberg SM. Hereditary cerebral amyloid angiopathy, piedmont type mutation. Neurol Genet 2020; 6: e411.

Ii Y, Maeda M, Ishikawa H, Ito A, Matsuo K, Umino M, et al. Cortical microinfarcts in patients with multiple lobar microbleeds on 3T MRI. J Neurol 2019; 266: 1887–96.

Linn J, Halpin A, Demaerel P, Ruhland J, Giese AD, Dichgans M, et al. Prevalence of superficial siderosis in patients with cerebral amyloid angiopathy. Neurology 2010; 74: 1346–50.

Linn J, Herms J, Dichgans M, Brückmann H, Fesl G, Freilinger T, et al. Subarachnoid hemosiderosis and superficial cortical hemosiderosis in cerebral amyloid angiopathy. AJNR Am J Neuroradiol 2008; 29: 184–6.

Love S, Chalmers K, Ince P, Esiri M, Attems J, Jellinger K, et al. Development, appraisal, validation and implementation of a consensus protocol for the assessment of cerebral amyloid angiopathy in post-mortem brain tissue. Am J Neurodegener Dis 2014; 3: 19–32.

Obici L, Demarchi A, de Rosa G, Bellotti V, Marciano S, Donadei S, et al. A novel AbetaPP mutation exclusively associated with cerebral amyloid angiopathy. Ann Neurol 2005; 58: 639–44.

Pichler M, Vemuri P, Rabinstein AA, Aakre J, Flemming KD, Brown RD, Jr, et al. Prevalence and natural history of Superficial Siderosis. A population-based study. Stroke 2017; 48: 3210–4.

Poels MM, Vernooij MW, Ikram MA, Hofman A, Krestin GP, van der Lugt A, et al. Prevalence and risk factors of cerebral microbleeds: an update of the Rotterdam scan study. Stroke 2010; 41: s103–6.

Premkumar DR, Cohen DL, Hedera P, Friedland RP, Kalaria RN. Apolipoprotein E-epsilon4 alleles in cerebral amyloid angiopathy and cerebrovascular pathology associated with Alzheimer's disease. Am J Pathol 1996; 148: 2083–95.

Schilling S, DeStefano AL, Sachdev PS, Choi SH, Mather KA, DeCarli CD, et al. APOE genotype and MRI markers of cerebrovascular disease: systematic review and meta-analysis. Neurology 2013; 81: 292–300.

Van Veluw SJ, Lauer A, Charidimou A, Bounemia N, Xiong L, Boulouis G, et al. Evolution of DWI lesions in cerebral amyloid angiopathy: evidence for ischemia. Neurology 2017; 89: 2136–42.

Van Veluw SJ, Reijmer YD, van der Kouwe AJ, Charidimou A, Riley GA, Leemans A, et al. Histopathology of diffusion imaging abnormalities in cerebral amyloid angiopathy. Neurology 2019a; 92: e933–e43.

Van Veluw SJ, Scherlek AA, Freeze WMT, Telgte A, van der Kouwe AJ, Bacskai BJ, et al. Different microvascular alterations underlie microbleeds and microinfarcts. Ann Neurol 2019b; 86: 279–92.

Xiong L, van Veluw SJ, Bounemia N, Charidimou A, Pasi M, Boulouis G, et al. Cerebral cortical microinfarcts on magnetic resonance imaging and their association with cognition in cerebral amyloid angiopathy. Stroke 2018; 49: 2330–6.